Available online at www.sciencedirect.com
ScienceDirect
Ceramics International 37 (2011) 3153–3160
CERAMICS INTERNATIONAL
www.elsevier.com/locate/ceramint

Synthesis and characteristics of nanocrystalline YSZ powder by polyethylene glycol assisted coprecipitation combined with azeotropic-distillation process and its electrical conductivity

Hong-Chang Yao, Xian-Wei Wang, Hao Dong, Rui-Rui Pei, Jian-She Wang, Zhong-Jun Li *

Department of Chemistry, Zhengzhou University, Zhengzhou 450001, PR China

Received 17 March 2011; accepted 16 May 2011
Available online 24 May 2011

Abstract

Nanoscale 8 mol% yttria stabilized zirconia (YSZ) powders were prepared by polyethylene glycol (PEG-1540) assisted coprecipitation coupling with azeotropic distillation drying process. The role of PEG and azeotropic-distillation on the morphology and particle size of YSZ was studied. Thermogravimetry and X-ray diffraction results showed that azeotropic-distillation could reduce the formation temperature of YSZ phase. X-ray patterns of the YSZ powders revealed that the crystallite size of the powders increases with increasing calcination temperature, which is consistent with transmission electron microscopy observations. The sintering behavior and the ionic conductivity of the pellets prepared from YSZ powders calcined at 800 °C were also studied. At sintering temperatures ≥1400 °C, more than 99% of the relative density was obtained. The alternating-current impedance spectroscopy results showed that the YSZ pellet sintered at 1450 °C has ionic conductivity of 0.0726 S cm^{-1} at 800 °C in air. The present work results have indicated that the PEG assisted coprecipitation combined with azeotropic-distillation drying process is an alternative method to synthesize yttria stabilized zirconia powders with a high sinterability and a good ionic conductivity.

Keywords: Yttria stabilized zirconia; Electrolyte; Nanoparticles; Azeotropic distillation; Polyethylene glycol

1. Introduction

Yttria stabilized zirconia (YSZ) is the most widely used electrolyte for solid oxide fuel cells (SOFCs) because of its high ionic conductivity, good mechanical strength and excellent chemical stability in both oxidizing and reducing environments [1–3]. However, YSZ, as a commonly used electrolyte material, has relatively high ionic conductivity only when operating at a temperature of about 1000 °C. Operation at such a high temperature limits the choice of stable materials for SOFC components and leads to degradation and sealing problems in devices. Hence, enormous efforts for the improvement of YSZ ionic conductivity at lower temperatures could be found in the literature. For example, Hui et al. [4] have recently reviewed various approaches to enhancing the ionic conductivity of polycrystalline zirconia-based oxide electrolytes in the light of composition, microstructure, and processing. According to Hui's opinion, the ionic conductivities of the YSZ electrolyte are not only influenced by the composition, but also influenced by the microstructure, and even processing conditions. The microstructures of YSZ electrolyte, i.e. the properties of grain and grain boundary, are primarily correlated to the quality of the starting powder such as particle size, surface morphology and homogenate. Therefore, many researches have focused on the preparation of homogeneous fine YSZ ceramic powders to maximize the electrolyte ionic conductivity.

Wet chemical approach is the most common methods to produce the nano-structured zirconia based ceramic powders due to its advantages such as atomic level doping and excellent control of stoichiometric homogeneity. Up to now, a number of wet chemical approaches for synthesizing nanocrystalline YSZ powders have been reported, such as spray drying [5], plasma spray [6], organic precursor route [7], homogeneous precipitation [8], sol–gel route [9], Pechini method [10],

* Corresponding author. Tel.: +86 371 6778 3123; fax: +86 371 6778 3123.
E-mail addresses: yaohongchang@zzu.edu.cn (H.-C. Yao), lizhongjun@zzu.edu.cn (Z.-J. Li).

0272-8842/$36.00
doi:10.1016/j.ceramint.2011.05.055

hydrothermal [11] and solvothermal synthesis [12]. Investigations indicated that the key to produce nanocrystalline YSZ powder was to prevent particle agglomeration in the process of formation of the precursors as well as the following drying step. Thus, various measures were introduced to deagglomerate, such as polymerized complex method [13] and balling milling method [5,7]. However, only a few researches paid attention to the effectiveness of deagglomeration treatment to the wet precursor particles for improving the property of the final product [9].

In the present study, we introduce a PEG assisted coprecipitation combining with an azeotropic-distillation process for the facile synthesis of nanocrystalline YSZ powder. Coprecipitation method is one of the widely adopted techniques for synthesis of nanocrystalline powder, but suffering from broad particle size distribution because of agglomeration. In order to alleviate agglomeration, polyethylene glycol (PEG-1540) as dispersant was employed to refine the grain size of the precursor and azeotropic distillation as drying technique was applied to reduce the formation of hard agglomeration in this work. It was found that the deagglomeration treatments were effective and weakly agglomerated and homogeneous YSZ nanoparticles could be obtained. The sinterability experiment and the ionic conductivity measurement of YSZ nanoparticles demonstrated that this method is an effective route to produce highly sinterable YSZ ceramic powders.

2. Experimental procedure

2.1. Material synthesis

Yttria stabilized zirconia nanoparticles were prepared *via* the coprecipitating route. $ZrOCl_2{\cdot}8H_2O$ and $YCl_3{\cdot}6H_2O$ were used as starting materials and dissolved in distilled water to form a solution (c_{total} = 0.4 mol L^{-1}), in which Zr^{4+} and Y^{3+} concentration met the formula of $(ZrO_2)_{0.92}(Y_2O_3)_{0.08}$. A given quantity of polyethylene glycol (PEG-1540) was added into the solution under vigorous stirring. Aqueous solutions of NH_4HCO_3 (0.4 mol L^{-1}) containing the appropriate amounts of PEG-1540 were also prepared. Simultaneously, two kinds of solutions were added dropwise into a four-neck angled round-bottom flask with two dropping funnels under stirring. The pH was controlled to keep to ~5.5 with ammonia (3.0 mol L^{-1}) during the process. After aging for 1 h, the precipitates were filtered and washed with distilled water till no Cl^- ions detectable ($AgNO_3$ test). Then, a small part of the as-prepared precursor was dried in air (denoted as **S1**) while the rest was transferred to flask, mixed with *n*-butanol and distilled to remove water as azeotrope. The dehydrated powder was further dried in a vacuum oven at 60 °C for more than 12 h (denoted as **S2**). The obtained powders were calcined at different temperatures for 2 h to examine the phase formation of YSZ. To examine the surfactant effects, control experiment with no PEG-1540 addition was conducted (the dehydrated powder was denoted as **S3**). The conversions of Zr^{4+} and Y^{3+} ions were analyzed by chemical titration method to the primary precipitate.

For fabricating an electrolyte, the powders calcined at 800 °C were uniaxially pressed (10 MPa) into compacts, and subsequently isostatically pressed at 180 MPa pressure. The shaped samples were sintered at different temperatures from 1250 °C to 1450 °C for 2 h in air for determining the optimum sintering temperature. The apparent densities of sintered pellets were determined using Archimedes principle.

2.2. Property measurements

X-ray powder diffraction (XRD) patterns of the resultant powders were recorded on an X-ray diffractometer (PANalytical X'Pert PRO, Netherlands) with Cu $K\alpha$ (λ = 0.15418 nm) at a step width of 0.03° and a scanning range of 10–70°. The mean crystallite size D was determined from diffraction line broadening using the Scherrer's formula ($D = \kappa\lambda/\beta\cos\theta$), where κ, λ, β, and θ are the Scherrer constant (κ = 0.9), the wavelength of Cu $K\alpha$ radiation, the full width at half maximum (FWHM) of the (1 1 1) reflection of YSZ phase, and the Bragg angle of the (1 1 1) reflection of YSZ phase, respectively.

The Brunauer–Emmett–Teller (BET) specific surface area was obtained *via* N_2 adsorption at 77 K (NOVA 1000e, Quantachrome Instruments, USA) and the measured result was translated into the equivalent particle size according to the equation: $D_{BET} = 6/(\rho S_{BET})$, where D_{BET} (nm) is the average particle size, S_{BET} is the specific surface area expressed in $m^2\ g^{-1}$, and ρ is the theoretical density of YSZ [5.9 g cm^{-3}]. The simultaneous Thermogravimetry and Differential Scanning Calorimeter (TG/DSC) were carried out using a thermal analyzer (Netzsch, STA 409 PC/PG) in a temperature range from room temperature to 800 °C at a heating rate of 10 °C min^{-1} in air atmosphere.

The size distribution and morphology of synthesized particles were observed using transmission electron microscopy (TEM, Tecnai G2 20, FEI Company, Netherlands). The microstructures of the sintered pellets were revealed by scanning electron microscopy (SEM, JSM-6700F).

2.3. Electrical measurements

Electrical conductivities of the sintered pellets were measured by using an impedance analyzer (PARSTAT 2273). The measurements were conducted in air in the temperature range from 250 to 1000 °C and in the frequency range from 0.1 Hz to 1 MHz. Curve fitting and resistance calculation were done by ZSimpWin software. The conductivities were calculated using the expression of $\sigma = l/SR$, where l is the sample thickness and S is the electrode area of the sample surface. Activation energies (E_a) were calculated by fitting the conductivity data to the Arrhenius relation for thermally activated conduction, which is given as: $\sigma T = \sigma_0 \exp(-E_a/kT)$, where σ, σ_0, E_a, k, and T are the conductivity, pre-exponential factor, activation energy, Boltzmann constant and absolute temperature, respectively.

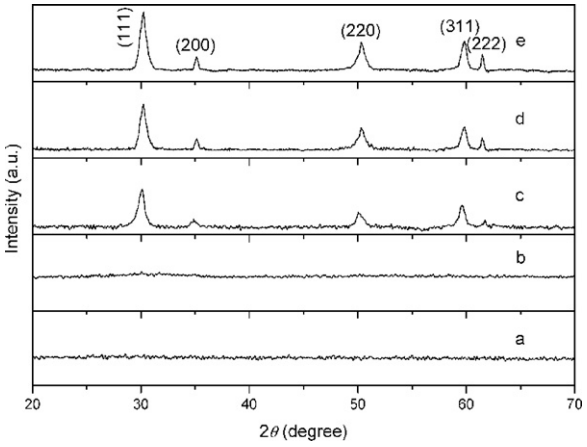

Fig. 1. XRD patterns of **S1** (a) and the YSZ powders calcined at 400 °C (b), 500 °C (c), 600 °C (d) and 800 °C (e) for 2 h.

3. Results and discussion

3.1. X-ray diffraction analysis

The XRD patterns of **S1**, **S2** and powders calcined at various temperatures are shown in Figs. 1 and 2, respectively. It can be seen that **S1** kept amorphous state till 400 °C while **S2** had transformed into YSZ phase at 400 °C. The result shows that azeotropic-distilling treatment can reduce the formation temperature of YSZ phase. The XRD peaks shown in Figs. 1 and 2 were rather broad, so it was difficult to distinguish between cubic and tetragonal structures. As the calcining temperature increased, however, a simultaneous narrowing of the peaks was observed. The average crystallite sizes of YSZ were calculated according to the Scherrer's equation. The typical crystallite sizes of **S2** calcined at 400, 600 and 800 °C was determined to be 7.8, 16.5 and 35.8 nm.

3.2. Thermal analyses

In order to further evaluate the crystallization behavior of the powders, TG/DSC curves of **S1** and **S2** were analyzed. The TG/DSC curve of **S1** (Fig. 3) shows that the total weight loss observed between 30 and 800 °C was about 35%. A pronounced endothermic peak near 106 °C was observed in the DSC curve. Afterwards, the precursor was progressively decomposed due to dehydroxylation with increasing temperature. The exothermal peak at 502 °C, accompanied by a weight loss (2.4%), may be attributed to fast formation and crystallization of amorphous zirconia or a rapid release of bound residual hydroxyl groups at the higher temperature.

The TG/DSC curve of **S2** shows a much less weight loss compared with that of **S1**, which may be attributed to the loss of water during the process of azeotropic distillation. There were two appreciable weight losses below 100 °C and 170 °C, accompanied with two endothermic peaks at 80 °C and 152 °C in the DSC curve, presumably due to the removal of absorbed water and *n*-butanol. The subsequent loss up to 400 °C was attributed to the remnant *n*-butanol. The weight loss tended to decrease with increase in reaction temperature. The weight change (∼2.2%) with exothermic peak at ∼445 °C may be also ascribed to the crystallization of YSZ phase and the release of leftovers of hydroxyl groups.

From the thermal analysis, it can be seen that the formation temperature of YSZ phase of **S2** decreased about 57 °C compared with that of **S1**. The result was in accordance with the XRD results, shown in Figs. 1 and 2.

3.3. Effect PEG dispersant and azeotropic distillation on grain size

Effects of ionic or non-ionic surfactant as deagglomerating reagent on the grain size are well known, as reported by Yao and Xie [14]. The polymeric distribution and its subsequent removal during thermal treatment are expected to control the particle growth and the final morphology of the particles. As far as PEG is concerned, the amphiphilic parts of PEG molecules can provide a steric hindrance effect with its hydrophobic ends adsorbed onto the particle surface while the oxyethylene chain stretching into water phase. The precipitated particles were embedded in the polymer matrix and the neighboring particles

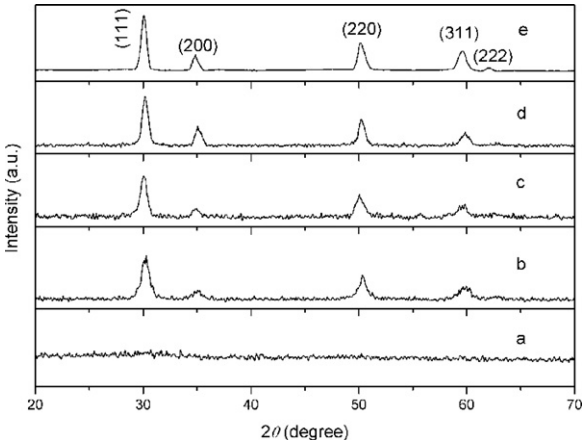

Fig. 2. XRD patterns of **S2** (a) and the YSZ powders calcined at 400 °C (b), 600 °C (c), 800 °C (d) and 1000 °C (e) for 2 h.

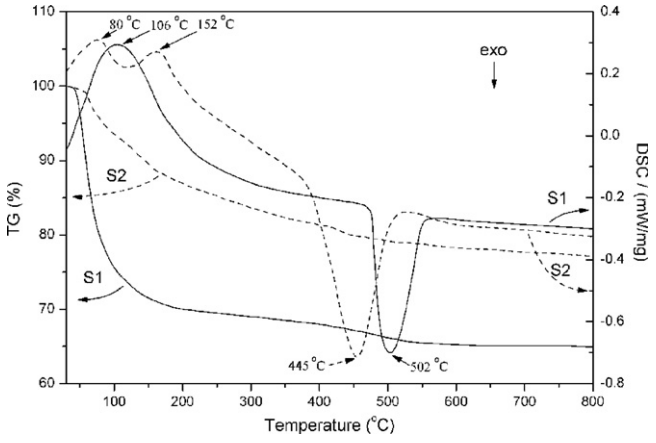

Fig. 3. TG/DSC curves of **S1** and **S2**.

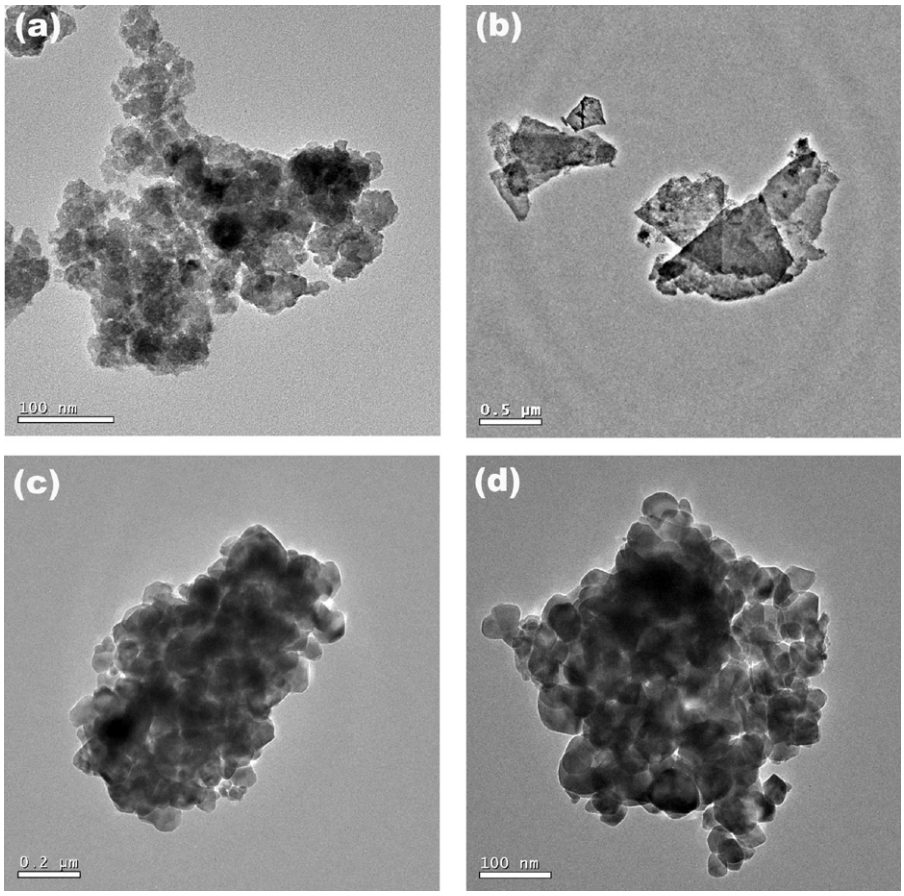

Fig. 4. TEM micrographs of **S1** (a), **S3** (b) and YSZ powders of **S3** (c) and **S1** (d) calcined at 600 °C.

were separated from each other. Thus the growth of the particles was suppressed. Fig. 4a shows the loose morphology of **S1**. On the other hand, **S3** with no PEG addition shows tight construction, as shown in Fig. 4b.

As expected, **S3** will be subjected to severe agglomeration during subsequently calcining step (Fig. 4c). However, it is unexpected that **S1** still suffered from obvious agglomeration during firing step (see Fig. 4d). The reason was to be explored and explained as follows. Since the product experienced a washing procedure, most of the surfactants adsorbed on the particle surfaces were rinsed out due to weak Van der Waals' forces between precipitates and PEG. Thus the dispersed particles got recongregated because of shrinking of elimination water molecules in the calcining step. In order to prevent recongregating during the drying process, azeotropic-distillation technique was introduced to reduce the surface tension of the particles.

Azeotropic-distillation technique has proved to be a quite efficient method to eliminate the residual water in the synthesis of yttria doped ceria electrolyte [15] and $La_{0.8}Sr_{0.2}MnO_{3-\delta}$ cathode [16]. Recently, Yao et al. [17] had successfully synthesized dense lanthanum silicate oxyapatite sintered ceramics with high conductivity by using this technique.

It is well known that hydrolysis of Zr(IV) occurred in strongly acidic solutions and was dominated by the formation of polymeric species such as $[Zr_4(OH)_8(H_2O)_{16}]^{8+}$ [18]. Thus the surface of zirconium hydrolysate is full of –OH groups and these –OH groups form extensive hydrogen bonds between particles. When these –OH groups were eliminated during the drying process, it would cause agglomeration. But when the azeotropic-distillation process was introduced, the –OH groups on the surface of the particles were replaced by $-OC_4H_9$ groups. Consequently, the possibility of the formation of strong chemical bonds and hard agglomerates were greatly eliminated.

Fig. 5 shows the morphologies of **S2** and the powders calcined at 400 °C, 600 °C and 800 °C. As can be seen, **S2** is composed of homogeneous nanoparticles. The extent of agglomeration of the particles is very weak after azeotropic distillation because the surface tension had been greatly reduced when the hydroxyl groups replaced by *n*-butanol (Fig. 5a). At the same time, these nanoparticles showed excellent non-agglomeration during the calcining step. Fig. 5b–d shows TEM morphologies of **S2** calcined at different temperatures. The average particle size was about 9, 15 and 38 nm for powders calcined at 400, 600 and 800 °C. The measured specific surface area of the 800 °C powder was measured to be 23.6 $m^2\ g^{-1}$ and the calculated particle size according to the equation $D_{BET} = 6/(\rho S_{BET})$ was 43.1 nm. The calculated particle size is comparable to that observed by TEM and in good agreement with that calculated from Scherrer's equation.

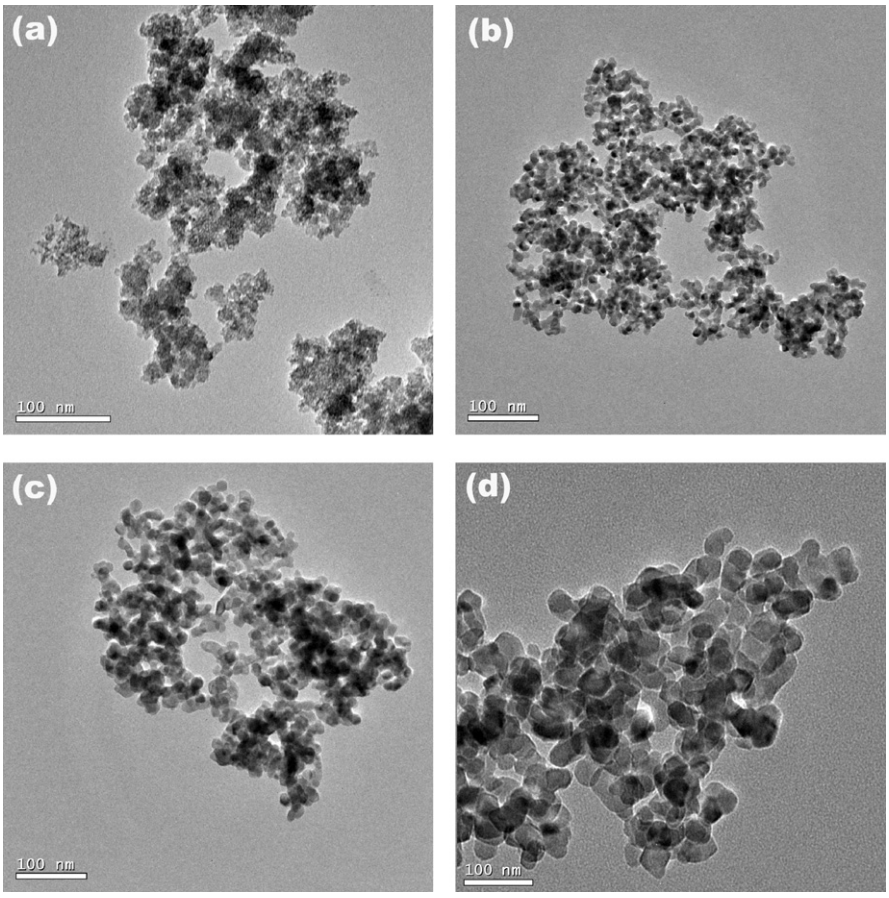

Fig. 5. TEM micrographs of **S2** (a) and the powders obtained by calcining the distilled powder at 400 °C (b), 600 °C (c) and 800 °C (d).

3.4. Sintering behavior

High green densities of over 48% relative density for **S2** calcined at 800 °C were obtained after isostatically pressing. Fig. 6 depicts the relative density as a function of sintering temperature of the obtained pellets. It was found that by increasing the sintering temperature, the relative density increased. The samples sintered at 1250 and 1450 °C have relative densities of 88.5% and 99.2%, respectively. These results were demonstrated by the microscopic observations. Fig. 7 shows three typical SEM micrographs of the cross section of the broken pellet samples sintered at 1250, 1350 and 1450 °C. Pores were clearly seen within the YSZ grains of the sample sintered at 1250 °C (Fig. 7a). When the sintering temperature increased to 1350 °C, the amount of pores decreased obviously, as illustrated in Fig. 7b. Further increase in sintering temperature leads to further eliminate pores and at last almost fully dense YSZ ceramic was made (Fig. 7c). High relative density may mean good ionic conductivity, as shown below.

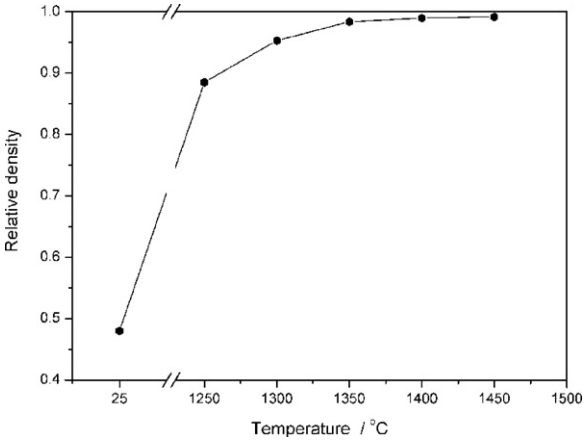

Fig. 6. Relative densities as a function of sintering temperatures of the sintered pellets.

3.5. Electrical properties

The electrical conductivities for the pellets prepared from **S2** sintered at different temperatures were measured and typical Nyquist impedance plots recorded in air at 300, 600 and 900 °C for the sample sintered at 1350 °C are shown in Fig. 8. The impedance spectra had been fitted and suitable equivalent circuits had been given in the inset of Fig. 8. It can be seen that at 300 °C, the impedance spectrum consisted of an uncompleted semicircle in the high frequency, a depressed semicircle in the middle frequency and a spike in the low-frequency. The uncompleted semicircle corresponded to the bulk impedance contribution and the semicircle was related to the grain

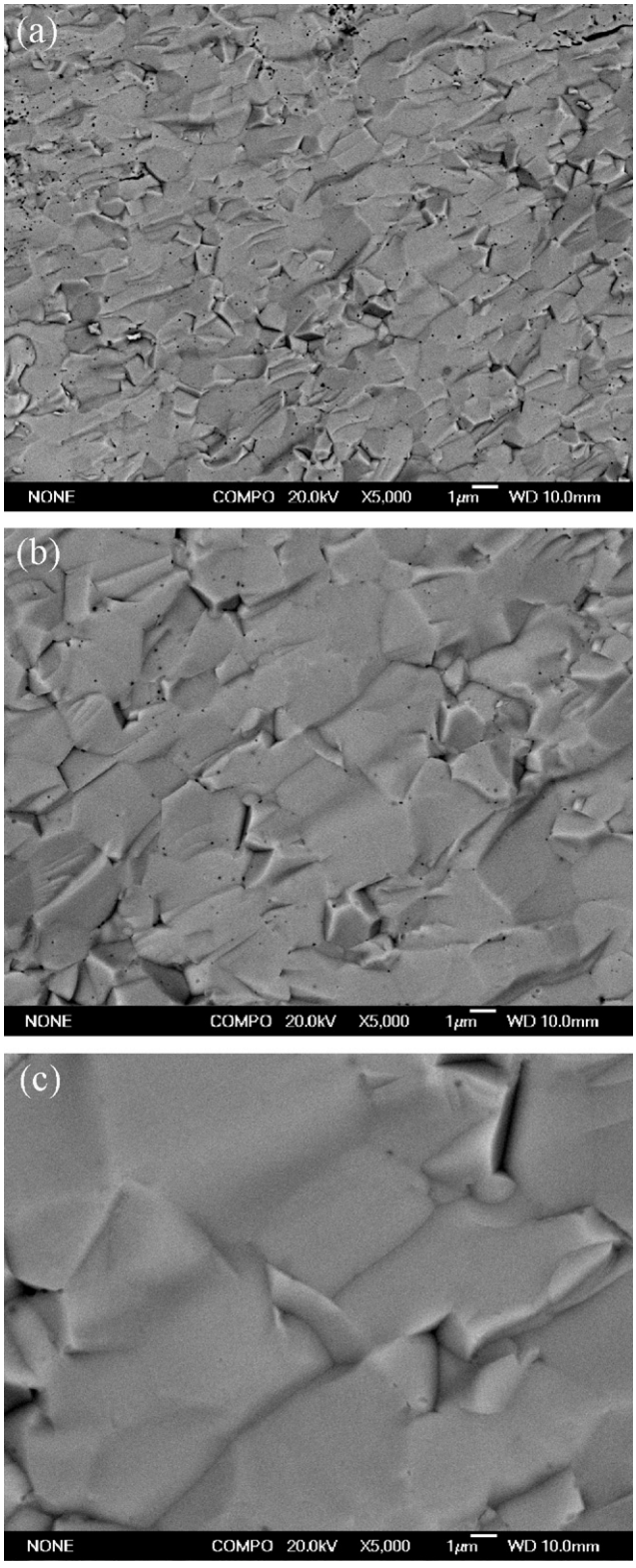

Fig. 7. SEM fractograph of the pellets sintered at 1250 °C (a), 1350 °C (b) and 1450 °C (c).

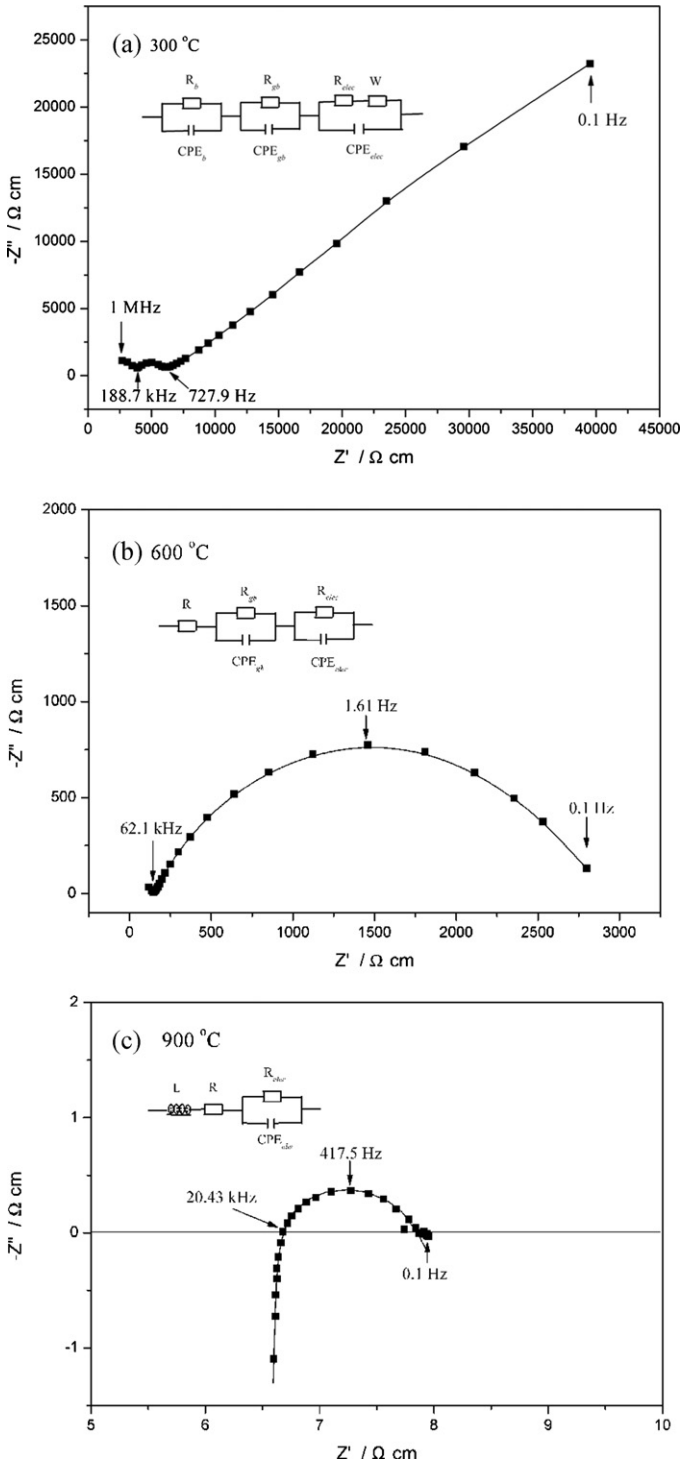

Fig. 8. Typical Nyquist plots recorded at (a) 300 °C, (b) 600 °C and (c) 900 °C for the sintered pellets prepared from powder calcined at 800 °C. The solid lines show the best fit using the equivalent circuits shown in the figures.

boundary. The spike inclined to the Z axis at roughly 45° indicated a Warburg impedance, according to Irvine [19]. The equivalent circuit including three serial R_i and $(CPE)_i$ parallels (i is b for bulk, gb for grain boundary or $elec$ for electrode, and CPE is a constant phase element) as well as a Warburg impedance (inset in Fig. 8a) was thus used to model the impedance spectrum using the software ZSimpWin. The least-squares fitting gave the capacitance values of the order of 10^{-12}, 10^{-9} and 10^{-5}, which corresponded to bulk, grain boundary and electrode–electrode interface effect, respectively. At

600 °C, the bulk and the grain boundary semicircle rapidly decreased and the spike turned into broad semicircle. The impedance data were thus modeled by a simplified equivalent circuit R(RQ)(RQ) (inset in Fig. 8b). Above 600 °C, the grain boundary semicircle was not observed either and the spike further collapsed to a semicircular arc. Additionally, there gradually emerged a large ''tail'' in the high-frequency region, which may be attributed to inductance of the experiment setup [20]. Therefore, the equivalent circuit LR(QR) (L is inductance) was used to fit the impedance spectrum.

As discussed above, however, it is very difficult to obtain both the bulk and the grain boundary resistances over the entire temperature range of investigation. Thus, the total resistances $R_t = R_b + R_{gb}$ were calculated and uniformly considered in this work. The total resistance was then converted to conductivity σ using the relation $\sigma = l/SR$.

Fig. 9 shows the plots of $\lg(\sigma T)$ versus $1/T$ for the pellets from **S2** and Table 1 lists the selected electrical conductivity and activation energy of the above samples. As shown in the figure and table, the total electrical conductivities increased with the increasing of the sintering temperatures, which can be probably attributed to the increment in their relative density. The electrical conductivity of YSZ can reach as high as 0.0726 S cm^{-1} at 800 °C, which is much higher than that synthesized by other method [21].

Another feature shown in Fig. 9 and Table 1 is that the Arrhenius plots showed curvatures at about 650 °C. The emergence of inflection points may be interpreted by the dissociation–migration energy model [22]. It is well known that partial substitution of Zr^{4+} with Y^{3+} ion will bring oxygen vacancies in the lattice because of the charge compensation, which could be expressed with following equations by using Kröger–Vink notation:

$$Y_2O_3 \xrightarrow{2ZrO_2} 2Y'_{Zr} + 3O_O^{\times} + V_O^{\bullet\bullet}$$

The vacancies ($V_O^{\bullet\bullet}$) induced by doping of aliovalent cations are not free but are bound to dopant cations to form defect associates ($Y'_{Zr}V_O^{\bullet\bullet}$) due to the coulombic attraction. The defect association might prevent oxygen vacancies from passing through the lattice. As the thermal dissociation of $Y'_{Zr}V_O^{\bullet\bullet}$ requires an additional energy to free oxygen vacancies, the activation energy thus includes dissociation energy E_a besides migration energy E_m. At high temperatures, however, all the oxygen vacancies are free and the activation energy reflects only the migration energy E_m of the oxygen vacancies. A critical temperature thus emerged. Table 1 shows the activation energy of YSZ electrolytes in the temperature range of 250–650 °C and 650–1000 °C, which means that the critical temperature is 650 °C. It can also be seen that the E_a values in the high temperatures are lower than those in the low temperatures, which is consistent with that the theory of the above dissociation–migration model.

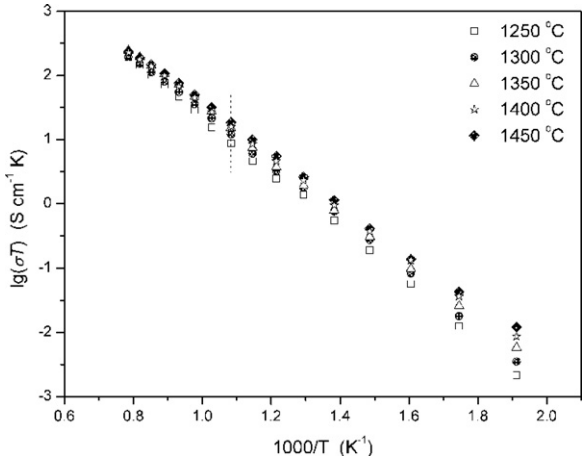

Fig. 9. Arrhenius plots of ionic conductivity of the pellets sintered at different temperatures.

Table 1
Total conductivity and activation energy of YSZ electrolyte sintered at different temperatures.

$T_{sintering}$ (°C)	Electrical conductivity, σ (S cm^{-1})			Activation energy, E_a (eV)	
	800 °C	900 °C	1000 °C	250–650 °C	650–1000 °C
1250	0.0492	0.095	0.157	0.846	0.795
1300	0.0586	0.105	0.173	0.866	0.754
1350	0.0674	0.122	0.191	0.850	0.740
1400	0.0669	0.124	0.205	0.922	0.786
1450	0.0726	0.131	0.213	0.866	0.747

4. Conclusions

Yttria stabilized zirconia powders were prepared using a PEG assisted coprecipitation combined with azeotropic-distillation route, in which a relative low calcination temperature was needed to form the single phase YSZ structure. The resulting powders exhibited a good sinterability and good electrical conductivity. For pellet sintered at 1450 °C, more than 99% of the relative density was obtained, and the maximum ionic conductivity of 0.0726 S cm^{-1} was measured at 800 °C in air. The results shows that the new developed approach of synthesizing YSZ powder is effective and the resulting YSZ ceramic has great potential to use as electrolyte for intermediate temperature solid oxide fuel cells.

Acknowledgements

We would like to thank the financial supports of the National Natural Science Found of China (Nos. 20971111, 21001096 and J0830412). Additionally, we thank the Student Research Training Program of Zhengzhou University for financial support.

References

[1] V.V. Kharton, F.M.B. Marques, A. Atkinson, Transport properties of solid oxide electrolyte ceramics: a brief review, Solid State Ionics 174 (2004) 135–149.

[2] J.W. Fergus, Electrolytes for solid oxide fuel cells, J. Power Sources 162 (2006) 30–40.
[3] D.J.L. Brett, A. Atkinson, N.P. Brandon, S.J. Skinner, Intermediate temperature solid oxide fuel cells, Chem. Soc. Rev. 37 (2008) 1568–1578.
[4] S. Hui, J. Roller, S. Yick, X. Zhang, C. Decès-Petit, Y. Xie, R. Maric, D. Ghosh, A brief review of the ionic conductivity enhancement for selected oxide electrolytes, J. Power Sources 172 (2007) 493–502.
[5] K. Prabhakaran, M.O. Beigh, J. Lakra, N.M. Gokhale, S.C. Sharma, Characteristics of 8 mol% yttria stabilized zirconia powder prepared by spray drying process, J. Mater. Process. Technol. 189 (2007) 178–181.
[6] Z. Wang, R. Hui, N. Bogdanovic, Z. Tang, S. Yick, Y. Xie, I. Yaroslavski, A. Burgess, R. Maric, D. Ghosh, Plasma spray synthesis of ultra-fine YSZ powder, J. Power Sources 170 (2007) 145–149.
[7] D.S. Patil, K. Prabhakaran, R. Dayal, C. Durga Prasad, N.M. Gokhale, A.B. Samui, S.C. Sharma, Eight mole percent yttria stabilized zirconia powders by organic precursor route, Ceram. Int. 34 (2008) 1195–1199.
[8] X. Xin, Z. Lü, Z. Ding, X. Huang, Z. Liu, X. Sha, Y. Zhang, W. Su, Synthesis and characteristics of nanocrystalline YSZ by homogeneous precipitation and its electrical properties, J. Alloys Compd. 425 (2006) 69–75.
[9] C.-W. Kuo, Y.-H. Shen, I.-M. Hung, S.-B. Wen, H.-E. Lee, M.-C. Wang, Effect of Y_2O_3 addition on the crystal growth and sintering behavior of YSZ nanopowders prepared by a sol–gel process, J. Alloys Compd. 472 (2009) 186–193.
[10] E.C. Grzebielucka, A.S.A. Chinelatto, S.M. Tebcherani, A.L. Chinelatto, Synthesis and sintering of Y_2O_3-doped ZrO_2 powders using two Pechini-type gel routes, Ceram. Int. 36 (2010) 1737–1742.
[11] Y.-C. Chang, M.-C. Lee, W.-X. Kao, T.-N. Lin, Preparation of a nanoscale/SOFC-grade yttria-stabilized zirconia material: a quasi-optimization of the hydrothermal coprecipitation process, Int. J. Appl. Ceram. Technol. 5 (2008) 557–567.
[12] Z. Hua, X.M. Wang, P. Xiao, J. Shi, Solvent effect on microstructure of yttria-stabilized zirconia (YSZ) particles in solvothermal synthesis, J. Eur. Ceram. Soc. 26 (2006) 2257–2264.
[13] S. Farhikhteh, A. Maghsoudipour, B. Raissi, Synthesis of nanocrystalline YSZ (ZrO_2–$8Y_2O_3$) powder by polymerized complex method, J. Alloys Compd. 491 (2010) 402–405.
[14] S.-Y. Yao, Z.-H. Xie, Deagglomeration treatment in the synthesis of doped-ceria nanoparticles via coprecipitation route, J. Mater. Process. Technol. 186 (2007) 54–59.
[15] S. Zha, Q. Fu, Y. Lang, C. Xia, G. Meng, Novel azeotropic distillation process for synthesizing nanoscale powders of yttria doped ceria electrolyte, Mater. Lett. 47 (2001) 351–355.
[16] J. Piao, K. Sun, N. Zhang, S. Xu, D. Zhou, Preparation and characterization of $La_{0.8}Sr_{0.2}MnO_{3-\delta}$ cathode for SOFCs fabricated using azeotropic distillation method, J. Rare Earths 24 (2006) 93–97.
[17] H.-C. Yao, J.-S. Wang, D.-G. Hu, J.-F. Li, X.-R. Lu, Z.-J. Li, New approach to develop dense lanthanum silicate oxyapatite sintered ceramics with high conductivity, Solid State Ionics 181 (2010) 41–47.
[18] J.R. Fryer, J.L. Hutchison, R. Paterson, An electron microscopic study of the hydrolysis products of zirconyl chloride, J. Colloid Interface Sci. 34 (1970) 238–248.
[19] J.T.S. Irvine, D.C. Sinclair, A.R. West, Electroceramics: characterization by impedance spectroscopy, Adv. Mater. 2 (1990) 132–138.
[20] E. Barsoukov, J.R. Macdonald, Impedance Spectroscopy: Theory, Experiment and Applications, John Wiley & Sons, Inc., 2005,, p. 246.
[21] Q. Wang, R. Peng, C. Xia, W. Zhu, H. Wang, Characteristics of YSZ synthesized with a glycine-nitrate process, Ceram. Int. 34 (2008) 1773–1778.
[22] C. Zhang, C.-J. Li, G. Zhang, X.-J. Ning, C.-X. Li, H. Liao, C. Coddet, Ionic conductivity and its temperature dependence of atmospheric plasma-sprayed yttria stabilized zirconia electrolyte, Mater. Sci. Eng. B 137 (2007) 24–30.